CuO decoration controls Nb_2O_5 photocatalyst selectivity in CO_2 reduction

André E. Nogueira,[1] Gelson T. S. T. Silva,[2,3] Jéssica A. Oliveira,[2,4] Osmando F. Lopes,[5,6] Juliana A. Torres,[2] Marcelo Carmo[6] and Caue Ribeiro[2,6*]

[1] *Department of Chemistry, Institute of Exact and Biological Sciences (ICEB), Federal University of Ouro Preto-UFOP, CEP: 35400-000, Ouro Preto - MG, Brazil*

[2] *Embrapa Instrumentation, Rua XV de Novembro, 1452, CEP: 13560-970, São Carlos - SP, Brazil.*

[3] *Department of Chemistry – Federal University of São Carlos, Via Washington Luiz, km 235, CEP: 13565-905, São Carlos - SP, Brazil.*

[4] *Department of Chemical Engineering – Federal University of São Carlos, Via Washington Luiz, km 235, CEP: 13565-905, São Carlos - SP, Brazil.*

[5] *Laboratory of Photochemistry and Materials Science, Institute of Chemistry, Federal University of Uberlândia, CEP: 38400-902, Uberlândia - MG, Brazil.*

[6] *Forschungszentrum Jülich GmbH, Institute of Energy and Climate Research (IEK-14): Electrochemical Process Engineering, 52425 Jülich, Germany.*

* Corresponding author: caue.ribeiro@embrapa.com.br

Tel.: +55 16 2107 2800; fax: +55 16 2107 2902

Abstract

The reform of CO_2 through photocatalytic processes to obtain products with high energy value and compatible with the current energy infrastructure, is a compelling strategy to minimize the emission of CO_2 at atmosphere, one of the main greenhouse gases. However, practical application of such a photocatalytic system requires significant efforts for improved CO_2 photoreduction performance and product selectivity. Thus, in the present work, CuO nanoparticles were combined with Nb_2O_5 in order to improve the photocatalytic properties of these semiconductors in the CO_2 photorreduction process. The Nb_2O_5/CuO heterojunctions were prepared via solvothermal treatment method, while that experimental tools, such as FESEM, HRTEM, and DRS were employed to evaluate the microstructural and electronic properties. We describe how CuO decoration over Nb_2O_5 adjusts its selectivity for CO_2 reduction to CH_4, HCOOH or H_3CCOOH in different contents. An investigation of CO_2 photoreduction using different electron donors/scavengers (water, sodium oxalate and potassium bromate) under ultraviolet radiation revealed that its decoration influences local CO production by modifying the selectivity. CO has been confirmed as the main intermediate for HCOOH and CH3COOH production, and CO_2 reduction efficiency increases with low CuO content (2.5% wt), leading to the formation of soluble hydrocarbons and increasing for CH_4 in higher amounts (10% wt).

Keywords: CO_2 photoreduction; artificial photosynthesis; heterojunction; mechanism; niobium oxide.

1. Introduction

CO_2 photoreduction, also known as artificial photosynthesis, is an alternative for hydrocarbon production as methane, methanol and formic acid[1-3], and also contributes to addressing energy and environmental issues. Although CO_2 photoreduction in water using semiconductors as photocatalysts has long been demonstrated[4], achievements in this area remain insignificant compared to that with other photoactivated reactions, such as H_2 production by water-splitting and pollutant photodegradation[5-7]. The main challenge lies in the high chemical stability of CO_2, implying that charge (e^-/h^+ pairs) recombination effects are maximized by poor electron transference to CO_2 during the reaction. Therefore, the catalysts must have low charge recombination rates and surface affinity for CO_2 in order to initiate the CO_2 reduction reaction[8].

Our research group recently demonstrated that pristine Nb_2O_5 has potential for CO_2 photoreduction, but with preferential CO evolution. Despite CH_4 being observed in specific synthesis conditions, its yields remain low, indicating that the interaction of CO_2 with Nb_2O_5 surfaces is limited by its high acidity[9-11]. Decorating the catalyst with other semiconductors may increase the interaction of reduction intermediates, modifying its selectivity. CuO is a viable choice due to its well-known ability to reduce CO_2 to CH_4. Furthermore, Nb_2O_5 forms with CuO a type-II heterostructure, that is, there is an overlap of the band gap's, which is possible due to the position of the semiconductor bands and due to their Fermi levels. In this type of configuration, semiconductor 1 has valence band and conduction band lower than the semiconductor 2. Therefore, electrons are accumulated in one semiconductor and holes in the other semiconductor, which causes the photogenerated charges to migrate in opposite directions, increasing the charge separation and favoring catalytic performance (adicionar as referencias)[12-14]. However, we recently found that CuO behaves as a co-reactant in CO_2 reduction, becoming poisoned after a few cycles[10]. Moreover, the synthesis method plays a critical role, small variations in particle size and surface chemistry can compromise the catalyst's performance[15]. We hypothesize that this instability is due to the associated oxidation reaction over the surface: when the electron-hole pair is formed, while electrons are used to reduce CO_2, the holes oxidize water into O_2 in the same particle, leading to further reactions that tend to induce poisoning. Therefore, charge separation is also crucial to maintaining CuO activity, which can be promoted through suitable heterojunction with other semiconductors[16-18].

Thus, in this paper we propose a Nb_2O_5/CuO heterojunction for CO_2 reduction tailored by solvothermal synthesis. This heterojunction has been successfully investigated for Cr(VI) reduction[19], which supports its potential for the more challenging CO_2 reduction process. The heterojunction increases catalyst selectivity. Furthermore, the mechanistic aspects of CO_2 reduction were properly evaluated. These results show that this heterojunction is an adequate photocatalyst for artificial photosynthesis, with a preference for CH_4 production and possible optimization for larger molecules such as HCOOH and CH_3COOH.

2. Materials and methods

2.1. Synthesis of the Nb_2O_5/CuO heterojunction (Nb/Cu)

Appropriate amounts of commercial Nb_2O_5 powder (Sigma-Aldrich, 99.9%) were dispersed in a copper acetate (Sigma-Aldrich, 99.0%) solution (0.05 M in ethanol-99.5%), with continuous stirring for 10 min, followed by solvothermal treatment at 110 ºC for 20 h. Nb/Cu samples were then prepared using differently weighted CuO ratios on Nb_2O_5 (between 2.5 and 10 wt%), with a constant total concentration in the solvothermal vessel of 2 $g.L^{-1}$. Following this treatment, samples were dried at 60 ºC for 4 h[19]. The samples prepared using weight ratios of CuO to Nb_2O_5 of 2.5, 5.0 and 10 wt% are denoted as Nb/Cu-2.5%, Nb/Cu-5% and Nb/Cu-10%, respectively.

2.2. Characterization

Basic characterization was performed by means of an X-ray powder diffractometer (XRD) with CuKα radiation (λ = 0.15406 nm), using a Shimadzu XRD 6000. Morphologies were analyzed by high-resolution transmission electron microscopy (HRTEM FEI TECNAI G2 F20) and field emission scanning electron microscopy (FESEM JEOL JSM 6701F). Samples for the HRTEM analysis were prepared by wetting the carbon-coated copper grids with a drop of the colloidal suspensions and air-drying. Semi-quantitative atomic compositions were achieved with energy-dispersive X-ray spectrometry (Gatan EDX accessory coupled to the HRTEM). Cu concentration in the heterostructures was analyzed through atomic absorption spectrophotometry (AAS Perkin Elmer PinAAcle 900T).

Specific surface areas (SSA) were established by measuring nitrogen adsorption/desorption isotherms at 77 K, using a Micromeritics ASAP-2020 instrument. Then, SSAs were calculated using the Brunauer-Emmett-Teller (BET) method. Diffuse

reflectance spectra (DRS) in the ultraviolet-visible region were recorded at between 200 and 800 nm at ambient temperature using a Varian Cary 5G instrument operating in diffuse reflectance mode and with the band gap energy determined by the Tauc method[20,21].

The characterization procedure using different techniques, such as X-ray diffractometry, diffuse reflectance spectroscopy, and XPS survey, as well as a graph showing the CO_2 concentration during the photoreduction process over time, is shown in detail in the Supporting Information.

2.3. Photoreduction tests

CO_2 photoreductions were carried out in a cylindrical steel reactor covered in borosilicate glass and with a 500 mL capacity. 0.3 g of each of the catalyst powders were dispersed in 300 mL of water. Ultrapure CO_2 was then bubbled through the open-top reactor for at least 20 min to ensure that all dissolved oxygen was eliminated. The pH of the solution after the CO_2 bubbling was approximately 5.5. The illumination system included a UVC lamp (OSRAM 11 W, with a maximum of 253.7 nm) in the center of the reactor and an incident light intensity of 21.49 $mW.cm^{-2}$. To better understand the reaction mechanism, CO photoreduction was carried out under the same conditions of CO_2 reduction, having only changed the bubbling gas.

Reactions were monitored by gas sampling in the reactor headspace (200 ml) at regular intervals. Gaseous products were determined employing gas chromatography (model CP-3800, Varian) using a thermal conductivity detector (TCD) and flame ionization detector (FID), with the analytical method temperature of 150 °C for FID, 200 °C for TCD, respectively, and the injector temperature of 150 °C. It was used a packaged column HayeSep N (0.5m × 1.8″) containing a 13X molecular sieve. High-performance liquid chromatography (HPLC) measurements were carried out to verify products formed in the liquid phase. Samples were collected after 24 h of the CO_2 reduction reaction and 20 µL were injected into the Shimadzu HPLC-LC-20AD chromatograph. Aminex HPX-87H column (300 × 7.8 mm) capable of analyzing carboxylic acids and alcohols was used, with dilute solution of H_2SO_4 (3.3 mmol L^{-1}) as mobile phase with 0.6 mL min^{-1} flow rate. Column and detectors were kept at 40 °C[15].

Reactions were monitored by gas sampling in the reactor headspace (200 ml) at regular intervals. Gaseous products were determined by means of gas chromatography using a thermal conductivity detector (TCD) and flame ionization detector (FID) Varian,

CP-3800. High-performance liquid chromatography (HPLC) measurements were carried out to verify products formed in the liquid phase. Samples were collected after 24 h of the CO_2 reduction reaction and 20 µL were injected into the Shimadzu HPLC-LC-20AD chromatograph[15]. Blank reactions were carried out to confirm that the measured CH_4 and CO were in fact derived from CO_2 photoreduction and not from previously dissolved gases or self-photolysis. The first blank reaction was performed without the catalyst, holding all other experimental conditions constant. The second test was conducted in a nitrogen atmosphere to verify any product release or formation from the catalyst.

3. Results and discussion

3.1. Characterization

The X-ray diffraction patterns are shown in **Figure 1** and identified by the Nb_2O_5 orthorhombic structure (JCPDS #71-0336) for both the pristine Nb_2O_5 and Nb_2O_5/CuO heterojunctions. CuO peaks are not present due to the low concentration (0-10%) and small particle sizes, despite the 2θ = 30-45° range (**Figure 1b**). Two main diffraction peaks of (-111) and (111) related to copper oxide (JCPDS #48-1548) are visible (see supplementary material). The effective CuO precipitation with the Nb_2O_5 phase is confirmed by atomic absorption spectrometry (**Table 1**) with values close to the expected compositions.

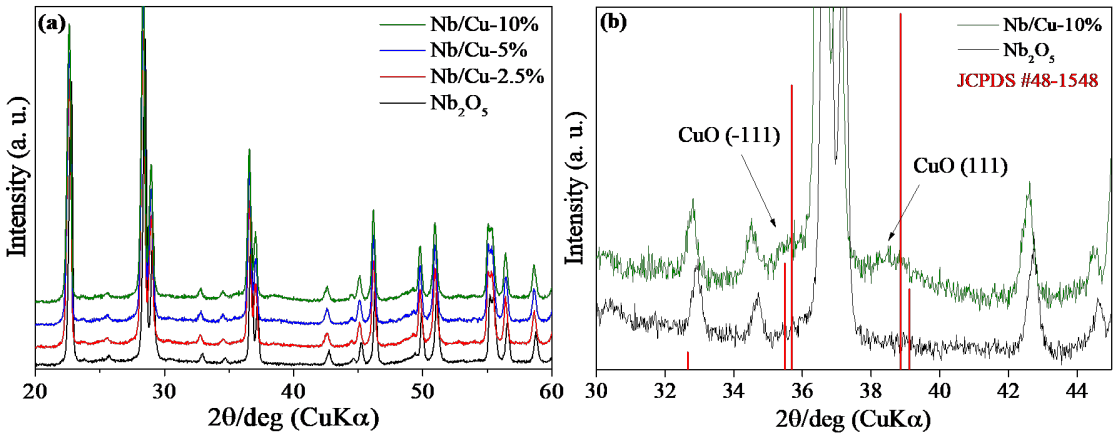

Figure 1. X-ray diffractions of the Nb_2O_5 and Nb_2O_5/CuO heterojunctions in the region between 15-65 (a) and 30-45 (b).

The optical properties of the composites were measured by UV-visible diffuse reflectance spectroscopy. The band gaps of the heterostructures were determined using

the Tauc model, assuming that CuO and Nb_2O_5 presented direct-type transition.[22,23] For their direct allowed band gap feature, the band gaps (E_g) of all synthesized samples were calculated according to the following formula:

$$\alpha h\nu = A(h\nu - E_g)^{1/2}, \quad (1)$$

where α is the linear absorption, A is a constant, $h\nu$ is the photon energy, and E_g is the direct band gap. Extrapolating the linear section of the $(h\nu) - (\alpha h\nu/A)^2$ to $(\alpha h\nu/A)^2 = 0$, the intercept value is E_g. UV-Vis spectra (**Figure S2**) indicate two band gaps, consistent with what is expected for the isolated phases, as can be seen in **Table 1** [22,23]. Specific surface areas (**Table 1**) increase with the CuO concentration, suggesting an increase in surface roughness from 1 to 8 $m^2.g^{-1}$.

Table 1. Band gap energy, Cu content (by AAS) and specific surface area (BET) for the synthesized materials.

Samples	Cu(%)	SSA ($m^2 \cdot g^{-1}$)	Band gap (eV)
Nb_2O_5	–	14	3.1
Nb/Cu-2.5%	2.91	1.0	2.1/3.1*
Nb/Cu-5%	5.55	4.1	2.2/3.1*
Nb/Cu-10%	8.18	8.4	2.2/3.1*
CuO	100	122	1.8

** The synthesized heterostructures showed two distinct bandgaps.*

Nb_2O_5 is composed of rods with an average particle size of 700 nm (**Figure 2a**), while the heterojunctions (Nb/Cu-2.5%, Nb/Cu-5% and Nb/Cu-10%, **Figure 2b-d**) randomly show CuO nanoparticles over the Nb_2O_5 surfaces. The interface between CuO nanoparticles and Nb_2O_5 is also displayed in **Figure 2e-f**). The interplanar spaces agree to (010) the Nb_2O_5 orthorhombic structure (0.38 nm) and (111) CuO monoclinic structure (0.24 nm)[24].

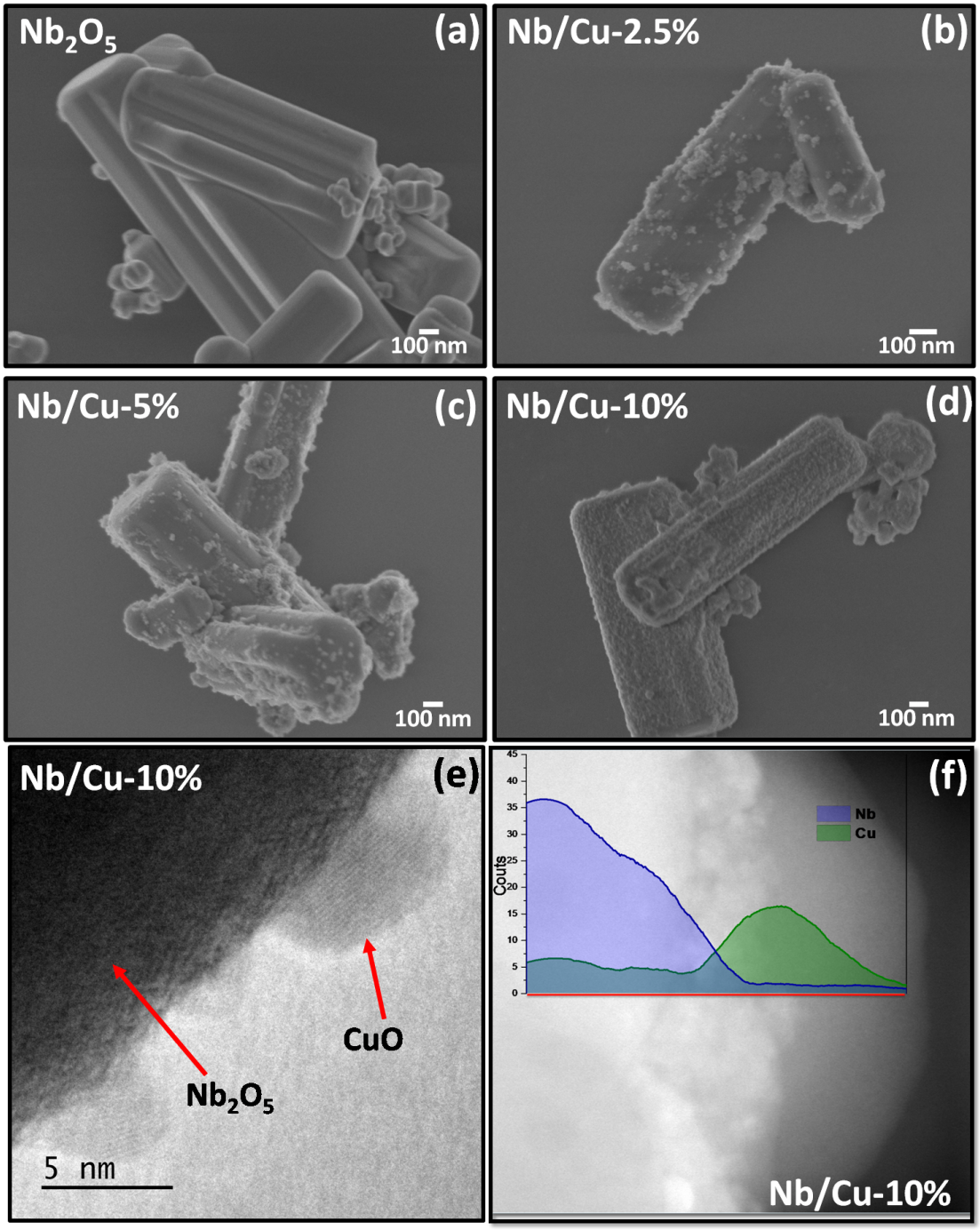

Figure 2. SEM micrographs of the Nb_2O_5 and Nb_2O_5/CuO heterostructures (a-d), HRTEM (e), and line scan for Nb and Cu elements (f) of the Nb/Cu-10% heterojunction.

The XPS survey analysis (**Figure S3**) shows that the Nb_2O_5 only has Nb signals, while the heterostructures present Cu signals, as expected. Through high resolution O1s XPS spectra (**Figure 3**), Nb_2O_5 displays two peaks at approximately 529.98 and 531.18 eV, respectively, related to oxygen coordinated with Nb and H (in OH)[25]. After the formation of the heterojunction between Nb_2O_5 and CuO, the peak intensity at 531.18 eV

increases with the CuO ratio, regarded to the binding energy contribution of intrinsic oxygen defects in CuO crystal lattice[26,27]. At 533.18 eV, the peak probably relates to O-C bonding from acetate groups on the copper oxide surface, as was previously reported by our research group[28].

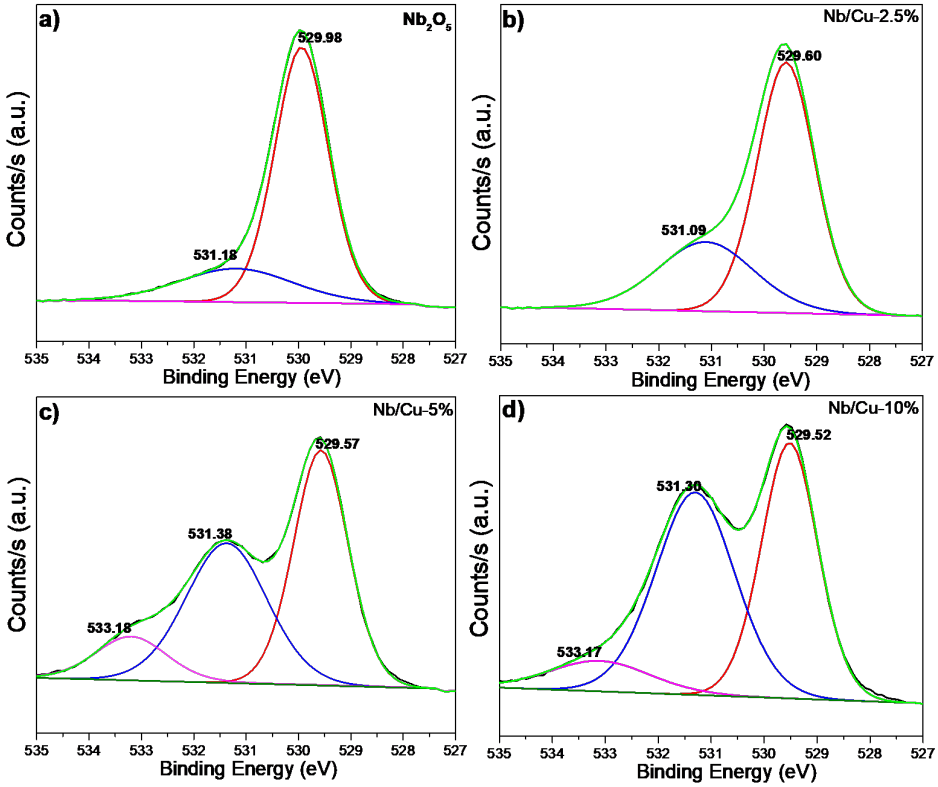

Figure 3. High-resolution XPS fitting of the O1s, a) Nb_2O_5, b) Nb/Cu-2.5%, c) Nb/Cu-5% and d) Nb/Cu-10%.

3.2. CO_2 photoreduction tests

Figure 4 shows CH_4 evolution profiles from CO_2 photoreduction, indicating that the Nb/Cu-10% heterostructure was more efficient than the other heterostructures – including Nb_2O_5 and TiO_2-P25 (as references). All of the heterojunctions were more active than the isolated Nb_2O_5 phase, indicating that the Nb_2O_5/CuO interaction probably increases charge carrier recombination time. CO_2 concentration in the reactor headspace is constant (**Figure S4**), indicating that photoreduction processes only take place in as-solubilized CO_2.

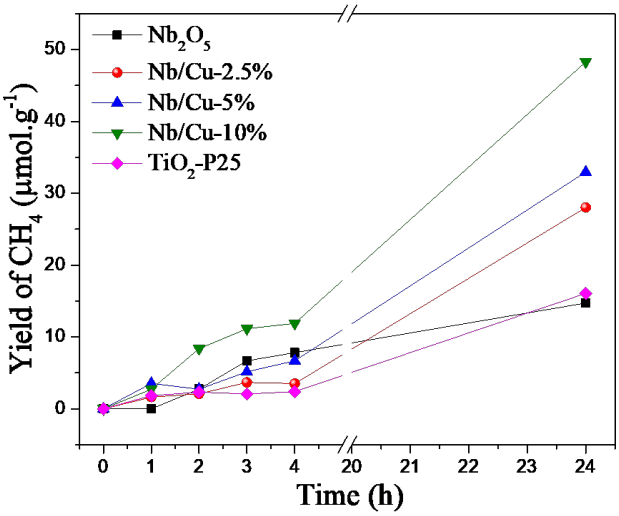

Figure 4. Kinetics of methane generation from the CO_2 photoreduction under UV irradiation at 25 ± 3 ºC.

The limits of the photoreaction can be probed by analyzing the reactions using scavengers that act as electron/hole sacrificial donors. O_2 is the only product, and at a remarkably high level, when CO_2 reduction is performed in a potassium bromate solution with a sacrificial electron scavenger inhibiting any CO_2 reduction (**Figure 5**). On the other hand, using sodium oxalate (a sacrificial electron donor), O_2 evolution from water is suppressed and, therefore, hydrogen will not be available for combining to form CO. In fact, analysis of the gas phase indicates that only CO was formed when the CO_2 photoreduction took place in the presence of sodium oxalate, as no hydrogen source was present. The imbalance between CO and CH_4 production suggests that other byproducts may be formed in solution by the interactions across both phases. In fact, some significant amounts of hydrocarbons in solution were detected by HPLC (**Figure 6a**) after 24 h of CO_2 reduction, mainly comprising formate ($HCOO^-$) and acetate (CH_3COO^-). The Nb/Cu-10% heterojunction was more active for $HCOO^-$ production while the Nb/Cu-2.5% heterojunction favored CH_3COO^-. These indicate that product formation depends on a balance with CO and CH_4 production, reinforcing that each phase in the heterostructure plays different roles in CO_2 reduction.

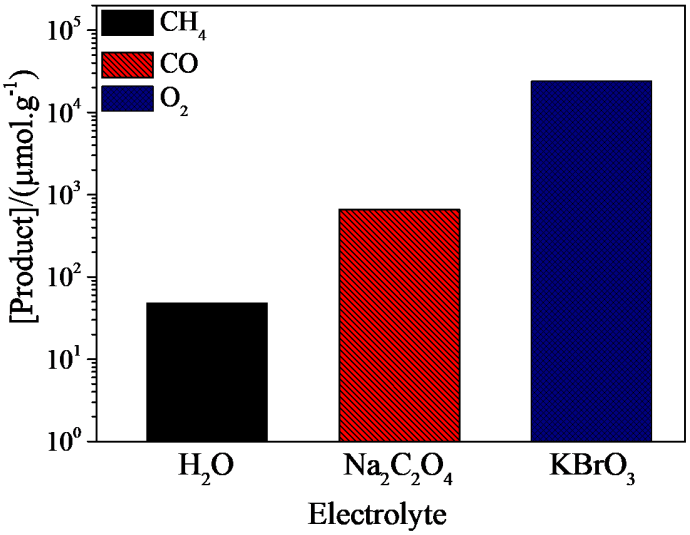

Figure 5. Influence of the electrolytes (H_2O, $Na_2C_2O_4$, and $KBrO_3$) on product selectivity in CO_2 photoreduction using the Nb/Cu-10% system.

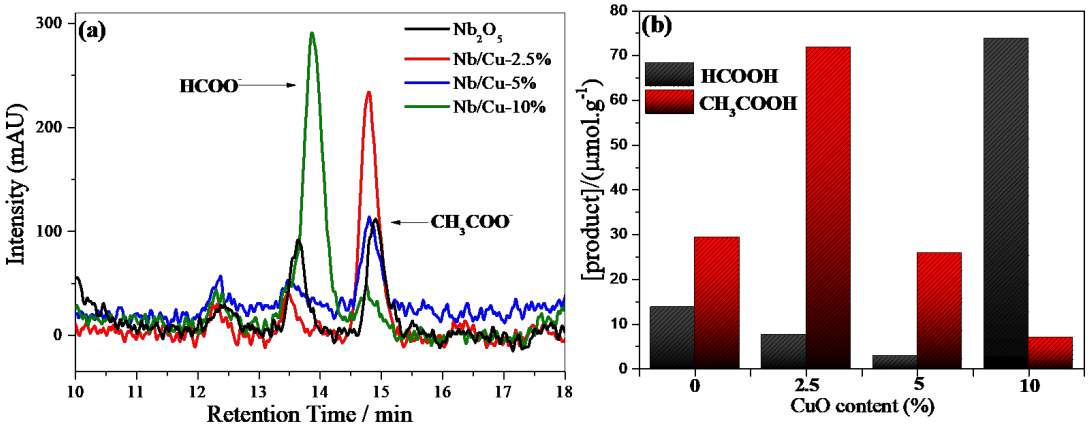

Figure 6. (a) Chromatogram and (b) quantification of products formed in solution after 24 h of reaction under UV radiation.

We can compare the efficiency of catalysts by considering the total CO_2 reduction efficiency, i.e., the effective number of electrons that the catalyst transferred for a reduced C species, as can be seen in **Table 2**. All of the CuO modifications increased Nb_2O_5 activity but the distribution of byproducts depends on the CuO content. We suspect that the CuO decoration favors the production of C-H bonds, which will influence in small contents to the dimerization of $–CH_3$ and –COOH groups, leading to H_3CCOOH production. In higher quantities (i.e., 10% CuO), the preference for CH_4 indicates that the catalytic behavior is dominated by CuO, which evenly covers all of the Nb_2O_5 surface. In

that sense, the capacity of the system to reduce CO_2 to CO is essential for increasing the formation of C2 molecules, even in the presence of CuO.

Table 2. Total production after 24 hours of reaction and CO_2 reduction efficiency.

Photocatalyst	Products (µmol/g)			*RE (n_{e^-}.g/µmol)
	CH_4	HCOOH	CH_3COOH	
Nb_2O_5	15	14	29.5	266
Nb/Cu-2.5 %	28	7.5	72	527
Nb/Cu-5.0 %	24	3.0	26	302
Nb/Cu-10 %	48	74	7	560

*RE-calculated by the total number of electrons used to reduce the CO_2.

Table 3. Apparent quantum yield calculated based on incident photons at 254 nm and the selectivity of the photocatalyst after 24 hours.

Photocatalyst	Apparent Quantum yield (%)			Selectivity (%)		
	CH_4	HCOOH	CH_3COOH	CH_4	HCOOH	CH_3COOH
Nb_2O_5	0.089	0.0208	0.175	45.1	10.5	44.4
Nb/Cu-2.5 %	0.166	0.0111	0.427	42.5	2.9	54.6
Nb/Cu-5.0 %	0.142	0.0044	0.154	63.6	2.0	34.4
Nb/Cu-10 %	0.285	0.110	0.0415	68.6	26.4	5.0

To confirm that CO is the reaction intermediate in accordance with the previous hypothesis, we performed a CO photoreduction experiment with an Nb/Cu-10% catalyst, as can be seen in **Figure 7**. As proposed, the CO photoreduction conducted to high formate and acetate yields compared to CO_2 photoreduction (only formate), confirming the dependence of CO availability for the formation of larger molecules. In fact, this was suggested by Jones et al.[29], who assert that stable CO_2 surface adsorption would preferentially lead to CH_4, while unstable adsorption may indicate fast CO desorption (assuming this as the first step of CO_2 photoreduction).

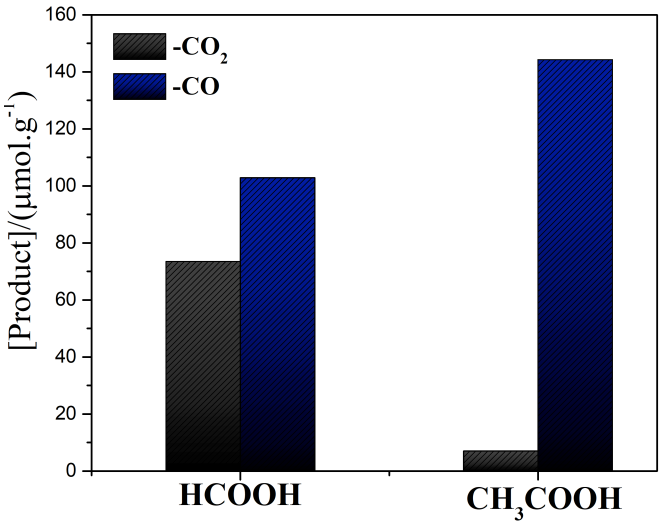

Figure 7. Performance comparison between CO_2 and CO photoreduction by the Nb/Cu-10% heterostructure.

In comparing this to a schematic band scheme for this heterojunction, it is apparent that both H_2O/O_2 evolution (+0.82 V vs NHE) and CO_2/CH_4 (-0.24 V vs NHE) can occur in both oxides, even when isolated[30]. However, the high band mismatch between CuO and Nb_2O_5 suggests that this system works as a *Z-scheme* instead of a real heterostructure, i.e., electrons preferentially migrate to CuO, favoring its reductive potential, while Nb_2O_5 concentrates holes, driving O_2 evolution (**Figure 8b**). Despite this remaining an open discussion as this point (depending on the detailed band structure characterization), the heterojunction is seen as being effective for promoting catalytic activity for reduction reactions **(Figure 8a)**.

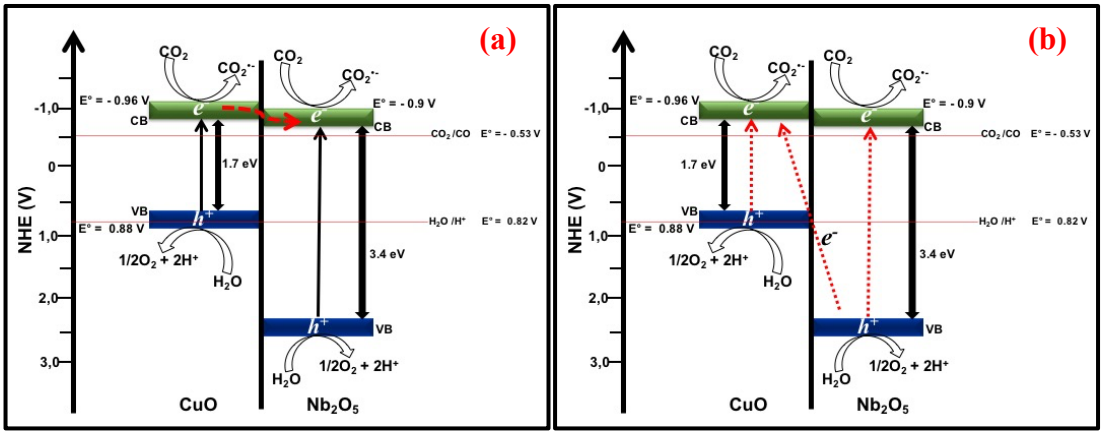

Figure 8. Scheme of energy levels in the formation of heterojunction (a) and Z-scheme (b) between CuO and Nb_2O_5, excited with UV radiation.

Based on these results, we can propose a general mechanism for the interaction of the catalyst surface with CO_2 and its relationship with the selectivity of the products generated in the CO_2 photoreduction process, as is shown in **Scheme 1**. Initially, we must take into account that, since the pH of the reaction medium is close to 5.5, a small part of the CO_2 molecules are in the form of HCO^{3-} ions, while the majority are in the form of CO_2. Although CO_2 is a linear molecule with no dipolar moment, both O atoms have a pair of electrons that can be transferred, so it can behave as a Lewis base; on the other hand, C can behave like a Lewis acid and receive a pair of electrons[31]. According to Nakajima et al.[32], the NbO_4 tetrahedron, present in the Nb_2O_5 structure, forms NbO_4-H_2O in the presence of water, which acts as Lewis acid sites receiving a pair of electrons from CO_2 oxygen, and so the oxygen from the CO_2 forms a predominant coordination with the surface of Nb_2O_5, whereas the surface of the CuO nanoparticles serve as Lewis base sites by donating a pair of electrons to the carbon atom, as demonstrated by Wu et al.[33]. Therefore, the increase in CH_4 production in accordance with the CuO content is consistent with a longer surface interaction with C, promoting subsequent interactions with H^+, as is also observed in the CO reduction experiment (**Figure 7a**). Similarly, the preferential CO production by Nb_2O_5 agrees with the lower C interaction in this oxide.

Scheme 1. Scheme of the possible CO_2 adsorption on the surfaces of Nb_2O_5 and CuO.

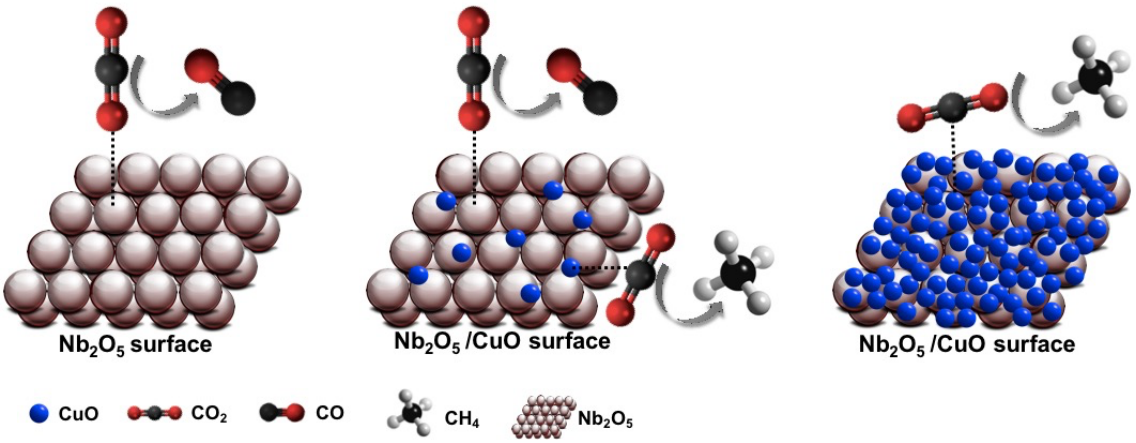

To investigate the catalyst's stability, Nb/Cu-10% was used four times, as is shown in **Figure 9**. The CO_2 photoreduction activity of Nb/Cu-10% decreased considerably in the first cycle, suggesting some poisoning. However, the heterojunction remained highly active over the next three cycles without any indication of subsequent poisoning. This suggests that the catalyst is reusable under the experimental conditions described, still offering significant CH_4 yields.

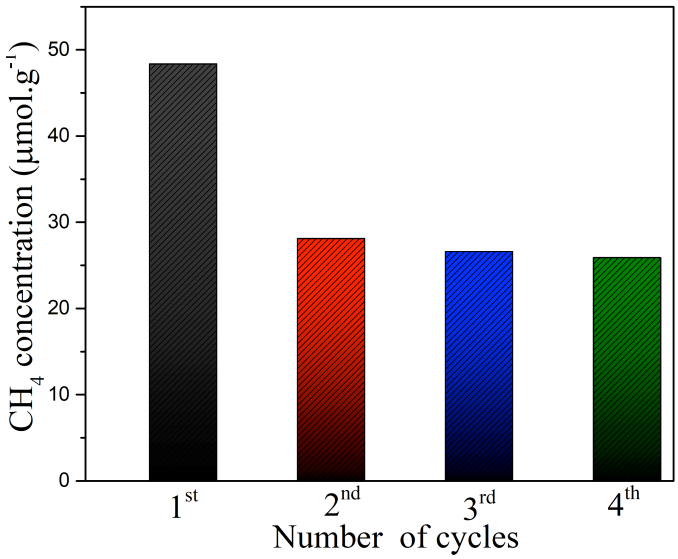

Figure 9. The cycling tests of the CO_2 photoreduction activity of Nb/Cu-10% after 24 h under UV irradiation.

Conclusions

CuO and Nb_2O_5 have both been shown to be viable photocatalysts for CO_2 reduction, leading to different byproducts (CH_4 and CO, respectively). The CuO decoration over Nb_2O_5 proposed herein, forming a heterojunction, can potentially increase the charge separation during photoexcitation but, more importantly, is influenced in the byproduct selectivity, increasing H_3CCOOH production with lower CuO contents. This mechanism study indicates that CO production is a key step in longer hydrocarbon production and is particularly important for H_3CCOOH – supporting the hypothesis that for this reaction, both $–CH_3$ and –CO should be formed on the same surface. These reactions can inform synthesis strategies for more efficient CO_2 → C2 reduction photocatalysts that make use of the specific activity of the different catalysts.

Acknowledgments

The authors are grateful to the Ministry of Science, Technology, and Innovation (through SisNANO Program – National System of Laboratories in Nanotechnology), the National Council for Scientific and Technological Development (CNPq, Brazil China Virtual Center in Nanotechnology Project and grant #402.287/2013-4, #407497/2018-8, and #159866/2018-9), Federal University of Ouro Preto-UFOP (grant nº. 23109.004080/2019-88), Coordination for the Improvement of Higher Education Personnel – Brazil (CAPES) - Finance Code 001, Sao Paulo Research Foundation

(FAPESP #15/14330-8, # 16/09746-3, #14/09014-7, and 2018/01258-5), and Embrapa Rede AgroNano for their financial support. Caue Ribeiro also acknowledges the Chinese Academy of Sciences (CAS) President's International Fellowship Initiative (PIFI) by financial support. We thank the Brazilian Nanotechnology Laboratory for Research in Energy and Materials (LNNano) and the Structural Characterization Laboratory (LCE) for technical support during the X-ray photoelectron spectroscopy (grant #13839) and transmission electron microscopy experiments, respectively.

References

1- Yuan, L.; Xu, Y.; Photocatalytic conversion of CO_2 into value-added and renewable fuels, Appl. Surf. Sci. **2015**, 342, 154-167. https://doi.org/10.1016/j.apsusc.2015.03.050.

2- Chang, X.; Wang, T.; Gong, J.; CO_2 photo-reduction: insights into CO_2 activation and reaction on surfaces of photocatalysts, Energy Environ. Sci. **2016**, 9 2177–2196. https://doi.org/10.1039/C6EE00383D.

3- Park, S.; Razzaq, A.; Park, Y.H.; Sorcar, S.; Park, Y.; Grimes, C.A.; In S. Hybrid Cu_x O−TiO_2 Heterostructured Composites for Photocatalytic CO_2 Reduction into Methane Using Solar Irradiation : Sunlight into Fuel. ACS Omega **2016**, 5, 868-875. https://doi.org/10.1021/acsomega.6b00164.

4- Inoue, T.; Fujishima, A.; Konishi, S.; Honda, K.; Photoelectrocatalytic reduction of carbon dioxide in aqueous suspensions of semiconductor powders, Nature. **1979**, 277, 637–638. https://doi.org/10.1038/277637a0.

5- Maeda, K.; Kazunari, D.; Photocatalytic Water Splitting: Recent Progress and Future Challenges, J. Phys. Chem. Lett. **2010**, 1, 2655–2661. https://doi.org/10.1021/jz1007966

6- Joy, J.; Jinu, M.; George, S. C.; Nanomaterials for photoelectrochemical water splitting e review, International Journal of Hydrogen energy **2018**, 43, 4804-4817. https://doi.org/10.1016/j.ijhydene.2018.01.099

7- Zheng, Y.; Pan, Z.; Wang, X. Advances in photocatalysis in China Chinese Journal of Catalysis **2013**, 34, 524–535. https://doi.org/10.1016/S1872-2067(12)60548-8

8- Das, S.; Daud, W.M.A.W. A review on advances in photocatalysts towards CO_2 conversion. RSC Advances **2014**, 20856–20893. https://doi.org/10.1039/c4ra01769b.

9- Silva, G.T.S.T.; Nogueira, A.E.; Oliveira, J.A.; Torres, J.A.; Lopes, O.F.; Ribeiro, C. Acidic surface niobium pentoxide is catalytic active for CO_2 photoreduction. Appl. Catal. B Environ. **2019**, 242, 349–357. https://doi.org/10.1016/j.apcatb.2018.10.017.

10- Nogueira, A. E.; Oliveira, J. A., da Silva, G.T.S.T.; Ribeiro, C. Insights into the role of CuO in the CO_2 photoreduction process. Scientific Reports, **2019**, 9, 1316 |https://doi.org/10.1038/s41598-018-36683-8

11- Cardoso, F.P.; Nogueira, A. E.; Patricio, P. S.; Oliveira L.C.A. Effect of tungsten doping on catalytic properties of niobium oxide. Journal of the Brazilian Chemical Society **2012**, 23, 702-709. https://doi.org/10.1590/S0103-50532012000400016

12- Mendonça, V. R.; Lopes, O. F.; Nogueira, A. E.; da Silva, G. T. S. T.; Ribeiro, C.; Challenges of Synthesis and Environmental Applications of Metal-Free Nano-heterojunctions, Nanophotocatalysis and Environmental Applications. **2019**. https://doi.org/10.1007/978-3-030-10609-6_4

13- Bueno, R. T.; Lopes, O. F.; Carvalho, K. T. G.; Ribeiro, C.; Mourão, H. A. J. L.; Semicondutores heteroestruturados: uma abordagem sobre os principais desafios para a obtenção e aplicação em processos fotoquímicos ambientais e energéticos, Quim. Nova, **2019**, 42, 661-675. https://doi.org/10.21577/0100-4042.20170372

14- Nogueira, A. E.; Ramalho, T. C.; Oliveira, L. C. A.; Photocatalytic Degradation of Organic Compound in Water using Synthetic Niobia: Experimental and Theoretical Studies. Topics in Catalysis **2011**, 54, 270-276. https://doi.org/10.1007/s11244-011-9641-x

15- Nogueira, André E.; da Silva, G. T.S.T.; Oliveira, J. A.; Torres, J. A.; da Silva, M. G.S., Carmo, M.; Ribeiro, C.; Unveiling CuO role in CO_2 photoreduction process – Catalyst or reactant? Catalysis Communications, **2020**, 137, 105929. https://doi.org/10.1016/j.catcom.2020.105929.

16- Li, X.; Liu, H.; Luo, D.; Li, J.; Huang, Y.; Li, H.; Fang, Y.; Adsorption of CO_2 on heterostructure CdS (Bi_2S_3)/TiO_2 nanotube photocatalysts and their photocatalytic activities in the reduction of CO_2 to methanol under visible light irradiation. Chem. Eng. J. **2012**, 180, 151–158. https://doi.org/10.1016/j.cej.2011.11.029.

17- Silva, G.T.S.T.; Carvalho, K.T.G.; Lopes, O.F.; Ribeiro, C. g-C_3N_4/Nb_2O_5 heterostructures tailored by sonochemical synthesis: Enhanced photocatalytic performance in oxidation of emerging pollutants driven by visible radiation. Appl. Catal. B Environ. **2017**, 216, 70–79. https://doi.org/10.1016/j.apcatb.2017.05.038.

18- Shi, W.; Chopra, N.; Nanoscale heterostructures for photoelectrochemical water splitting and photodegradation of pollutants. Nanomaterials and Energy, **2013**, 2, 158-178. https://doi.org/10.1680/nme.13.00009

19- Nogueira, A.E.; Lopes, O.F.; Neto, A.B.S.; Ribeiro, C. Enhanced Cr(VI) photoreduction in aqueous solution using Nb_2O_5/CuO heterostructures under UV and visible irradiation. Chem. Eng. J. **2017**, 312, 220–227. https://doi.org/10.1016/j.cej.2016.11.135.

20- Wood, D.L.; Tauc, J. Weak Absorption Tails in Amorphous Semiconductors, Phisical Rev. B. **1972**, 5. https://doi.org/10.1103/PhysRevB.5.3144

21- Varga, L.T.K.M.D.; Validity limits of Kubelka – Munk theory for DRIFT spectra of photodegraded solid wood, Wood Science and Technology **2011**, 45, 135–146. https://doi.org/10.1007/s00226-010-0314-x.

22- Ferraz, N. P.; Marcos, F. C. F.; Nogueira, A. E.; Martins, A. S.; Lanza, M. R.V.; Assaf, E. M.; Asencios, Y. J.O.; Hexagonal-Nb_2O_5/Anatase-TiO_2 mixtures and their applications in the removal of Methylene Blue dye under various conditions, Materials Chemistry and Physics, **2017**, 198, 331-340. https://doi.org/10.1016/j.matchemphys.2017.06.029

23- Radhakrishnan, A.A.; Beena, B.B. Structural and Optical Absorption Analysis of CuO Nanoparticles, Indian Journal of Advances in Chemical Science, **2014**, 2 158–161.

24- Chen, W.; Zhang, H.; Ma, Z.; Li, Z. High electrochemical performance and lithiation-delithiation phase evolution in CuO thin films for Li-ion storage, J. Mater. Chem. A Mater. Energy Sustain. **2015**, 3,14202–14209. https://doi.org/10.1039/C5TA02524A.

25- Qamar, M.; Abdalwadoud, M.; Ahmed, M. I.; Azad A.-M.; Merzougui, B.; Bukola, S., Yamani, Z. H.; Siddiqui, M. N.; Single-Pot Synthesis of (001)-Faceted N-doped Nb_2O_5/Reduced Graphene Oxide Nanocomposite for Efficient Photoelectrochemical Water Splitting. ACS Appl. Mater. Interfaces **2015**, 32, 17954-17962. https://doi.org/10.1021/acsami.5b04667

26- Biesinger, M. C. Advanced analysis of copper X-ray photoelectron spectra. Surf. Interface Anal. **2017**, 49, 1325-1334. https://doi.org/10.1002/sia.6239

27- Devadoss, A.; Sudhagar, P.; Ravidhas C.; Hishinuma, R., Terashima, C., Nakata K.; Kondo, T.; Shitanda, I.; Yuasa, M.; Fujishima, A.; Simultaneous glucose sensing and biohydrogen evolution from direct photoelectrocatalytic glucose oxidation on robust Cu_2O–TiO_2 electrodes, Phys. Chem. Chem. Phys., **2014**, 16, 21237. https://doi.org/10.1039/C4CP03262D.

28- Nogueira, A. E.; Giroto A. S., Neto, A. B.S., Ribeiro, C.; CuO synthesized by solvothermal method as a high capacity adsorbent for hexavalent chromium, Colloids and Surfaces A: Physicochemical and Engineering Aspects, **2016**, 498, 161-167. https://doi.org/10.1016/j.colsurfa.2016.03.022.

29-Jones, J.-P.; Prakash, G.K.S.; Olah, G.A.; Electrochemical CO_2 Reduction: Recent Advances and Current Trends, Isr. J. Chem. **2014**, 54, 1451–1466. https://doi.org/10.1002/ijch.201400081.

30- Lingampalli, S.R.; Ayyub, M.M.; Rao, C.N.R.; Recent Progress in the Photocatalytic Reduction of Carbon Dioxide, ACS Omega. **2017**, 2, 2740–2748. https://doi.org/10.1021/acsomega.7b00721.

31-Xin, C.; Hu, M.; Wang, K.; Wang, X.; Significant Enhancement of Photocatalytic Reduction of CO_2 with H_2O over ZnO by the Formation of Basic Zinc Carbonate, Langmuir **2017**, 27, 6667-6676. https://doi.org/10.1021/acs.langmuir.7b00620

32-Nakajima, K.; Baba, Y.; Noma, R,; Kitano, M.; Kondo, J. N.; Hayashi, Sh.;, Hara, M.;, $Nb_2O_5.nH_2O$ as a Heterogeneous Catalyst with Water-Tolerant Lewis Acid Sites, J. Am. Chem. Soc. **2011**, 133, 4224–4227. https://doi.org/10.1021/ja110482r

33- Wu, H.; Zhang, N.; Cao, Z.;, Wang, H.; Hong, S.; The Adsorption of CO_2, H_2CO_3, HCO_3^- and CO_3^{2-} on Cu_2O (111) Surface: First-Principles Study, International Journal of Quantum Chemistry, **2012**, 12, 2532-2540. https://doi.org/10.1002/qua.23250